International Journal of Pharmaceutics 411 (2011) 178–187

Contents lists available at ScienceDirect

International Journal of Pharmaceutics

journal homepage: www.elsevier.com/locate/ijpharm

Pharmaceutical Nanotechnology

Characterization of rhodamine loaded PEG-g-PLA nanoparticles (NPs): Effect of poly(ethylene glycol) grafting density

Sherief Essa, Jean Michel Rabanel, Patrice Hildgen*

Department of pharmaceutics, Universite de Montreal, C.P. 6128, succursale centre-ville, Montréal, Québec, Canada H3C 3J7

ARTICLE INFO

Article history:
Received 2 November 2010
Received in revised form 6 January 2011
Accepted 21 February 2011
Available online 31 March 2011

Keywords:
Nanoparticles
PEG-PLA
Grafting density
Rhodamine
Macrophage
Plasma proteins

ABSTRACT

In our previous study, PEG-g-PLA nanoparticles were developed and characterized. The aim of the present work is to investigate the effect of PEG grafting density (% PEG inserted onto poly(D, L)-lactide, PLA backbone) on both physicochemical and biological properties (mainly plasma protein binding and in vitro macrophage uptake) of PEG-g-PLA NPs. Rhodamine B (RHO) loaded NPs were prepared from a 1:1 (wt/wt) blend of PLA and PEG-g-PLA copolymer of varying PEG grafting density (1, 7, or 20% mol/mol of lactic acid monomer) by an o/w emulsion solvent evaporation method. These NPs were characterized with regard to their morphology, size, surface charge, loading efficiency, and rhodamine release. The extent of protein adsorption to the surface of different NPs was qualitatively investigated by dynamic light scattering technique. Additionally, the in vitro macrophage uptake following incubation of RAW 264.7 cells with rhodamine loaded PEG-g-PLA and PLA particles was investigated by confocal laser scanning microscopy (CLSM). The amount of NPs phagocytosed following incubation of RAW 264.7 cells with different concentrations of rhodamine loaded PLA or pegylated NPs for 24 h at 37 °C was also determined by fluorescence spectroscopy. ALL lyophilized NPs showed larger diameter in the range of 300–400 nm compared to freshly prepared NPs suspension indicating particle aggregation upon lyophilization. % EE of rhodamine was found to be between 10% and 68% wt/wt depending on PEG grafting density. The higher the grafting density of PEG over PLA backbone, the more the entrapment efficiency. All pegylated NPs showed low zeta potential (close to zero) values. In vitro release analysis revealed that rhodamine leaked from all nanoparticles at a very slow rate at physiological pH, thus making it suitable for both imaging and uptake studies with RAW 264.7 cells. All PEG-g-PLA NPs of different PEG grafting density were well tolerated and exhibited no toxicity to RAW 264.7 cells as seen by cell proliferation assays. Cellular uptake of NPs was mainly dependent on polymer type as well as PEG grafting density. Grafted copolymer NPs resulted in lower degree of macrophage uptake compared to PLA NPs in macrophages cell lines. The higher the PEG grafting density, the lower the uptake of NPs by macrophage cells. Minimum NPs uptake for all the investigated concentrations was achieved when the PEG grafting density was 7% mol/mol of lactic acid. When increasing the PEG grafting density in the nanoparticles above 7%, no significant reduction in NPs phagocytosis was achieved. Thus, this study shows that the optimal PEG density required for designing stealth PEG-g-PLA NPs suitable for drug delivery applications might vary from 4 to 7%.

1. Introduction

Biodegradable nanoparticles are promising carriers to improve the administration of certain drugs, vaccines, nucleic acid and therapeutic proteins (Cohen et al., 2000; des Rieux et al., 2006; Hans and Lowman, 2002; Soppimath et al., 2001). Benefits offered by biodegradable nanoparticles include improved therapeutic efficiency, enhanced protection of the active moiety from degradation, maintenance of drug concentrations within acceptable therapeutic limits, the need for fewer doses thus reducing dose-limiting side effects, prolonged biological activity, and finally better patient compliance (Panyam and Labhasetwar, 2003; Wang et al., 2007).

Poly(lactic acid) (PLA) or poly(lactide-co-glycolide) are the most widely used polymers in drug delivery systems. However, NPs formulated using either PLA or PLGA might suffer many drawbacks as their rapid uptake by the reticuloendothelial system after intravascular administration, low drug loading efficiency, inability to encapsulate a wide range of drugs particularly hydrophilic drugs, and in many cases inability to release their payload completely (Delie et al., 2001). Low drug incorporation of PLGA and PLA usually leads to large drug loss during NP formulation, and hence, encapsulating insufficient drug amounts for therapeutic efficacy (Govender et al., 1999; Leo et al., 2004). The former situation necessitates the use of high polymer levels that might exceed their safety

* Corresponding author. Tel.: +1 514 343 6448; fax: +1 514 343 6871.
E-mail address: Patrice.hildgen@umontreal.ca (P. Hildgen).

0378-5173/$ – see front matter © 2011 Elsevier B.V. All rights reserved.
doi:10.1016/j.ijpharm.2011.02.039

profile. Another drawback of PLGA and PLA is that an initial burst release of drug can be observed in most loaded NPs, which may result in a loss of much of the therapeutic dose before the target site is reached by the NPs (Magjarevic et al., 2008; Mohanraj and Chen, 2007). With these drawbacks of PLGA/PLA, a novel biodegradable polymer, PEG-g-PLA was early developed by our group (Nadeau et al., 2005). Our previous work focused mainly on the development and characterization of functionalized poly(D, L)-lactide (PLA) nanoparticles in order to improve the drug delivery behavior of PLA nanoparticles (Essa et al., 2010a,b). Functionalized poly(D, L)-lactide (PLA) nanoparticles development mainly depend on introducing a flexible moiety onto PLA hydrophobic cores in attempt to improve the drug delivery properties of the obtained NPs. A variety of pendant substituents could be grafted onto PLA to generate polymers of different physicochemical properties and hence different drug incorporation behavior than PLA itself. In the same work, we have reported the development and characterization of PEG-g-PLA NPs with some optimal properties ideal for drug delivery applications. Those properties were uniform size with narrow size distribution (~150–200 nm), neutral surface charge, higher encapsulation efficiency, and finally their ability to control the release of the entrapped model drug, ibuprofen for a period of 2 weeks.

In this part, we are attempting to study the effect of PEG grafting density over PLA backbone on the properties of PEG-g-PLA NPs either physicochemical or biological properties mainly in vitro plasma protein adsorption and macrophage cellular uptake. Another aim is to investigate the optimal PEG grafting density required to develop stealth particles from such type of grafted copolymers. In order to reach these goals, we prepared NPs encapsulating rhodamine B (RHO) as a fluorescent marker using grafted pegylated polymer; PEG-g-PLA with different PEG grafting densities (1, 7, or 20% mol/mol of lactic acid monomer). RHO was loaded into NPs in order to have labeled formulations suitable for investigating the cellular uptake of NPs by macrophage cell lines, RAW 264.7. It is important that the marker used is incorporated into the NPs at a sufficient level to give good detection by the used analytical methods. Thus, a 1:1 wt/wt blend of PLA: PEG-g-PLA of different PEG density was used to efficiently entrap RHO into NPs matrix. An o/w emulsion solvent evaporation method was used to prepare RHO loaded NPs. RHO should remain associated with the NPs so that we follow the fate of the NPs rather than the marker itself. Accordingly the drug incorporation and release of the marker from NPs were determined.

2. Material and methods

2.1. Materials

D, L-Lactide, poly(ethylene glycol) methyl ether (MePEG; 2000 Da), allyl glycidyl ether, tetraphenyltin, polyvinyl alcohol (PVA, average *M*w 9000–10,000 Da, 80% hydrolyzed), borane–tetrahydrofuran complex (1 M), acetone, toluene, pyridine, chloroform, thionyl chloride, rhodamine B (RHO), and albumin bovine were purchased from Aldrich Chemical Company Inc., Milwaukee, USA. Sodium hydroxide pellets were purchased from Anachemia Canada Inc. and dichloromethane (DCM) was purchased from Laboratoire Mat Inc., Montreal, Quebec, Canada. Fetal bovine serum and all other materials for cell culture were purchased from Invitrogen (Burlington, ON, Canada) unless otherwise stated.

2.2. Synthesis of polymers

Poly(D, L)-lactide (PLA) was synthesized by ring-opening polymerization of dilactide in argon atmosphere, using tetraphenyltin as the catalyst. Briefly, dilactide was crystallized from toluene solution and dried under vacuum before use. A weighed amount of purified dilactide was then placed in a round-bottom flask and purged thoroughly with argon. Bulk polymerization was carried at 180 °C for 6 h. The polymer thus obtained was dissolved in acetone and was purified by precipitating in water.

Polymer with poly(ethylene glycol)-grafted randomly on poly(D, L)-lactide (PEG7%-g-PLA) (PEG; *M*w 2000 Da) was synthesized as reported earlier (Nadeau et al., 2005). Briefly, D, L-dilactide (21.5 g, 93 mol%) was polymerized in the presence of allyl glycidyl ether (2.6 g, 7 mol%) with tetraphenyltin as the catalyst (1:10,000 mol with regards to D, L-dilactide) at 180 °C for 6 h under argon. Polylactic acid with allyl groups was purified by dissolving in acetone and precipitating in water. The allyl groups were converted to hydroxyl groups by hydroboration with an equimolar quantity of borane in tetrahydrofuran, followed by oxidation in the presence of hydrogen peroxide under alkaline conditions (1.5 mol of 3 N sodium hydroxide). The hydroxyl groups were oxidized to carboxylic acid groups using Jones reagent, which was further converted to an acid chloride using thionyl chloride (1:1000 M). Finally, methoxy-PEG was grafted onto the polymer backbone by the reaction between acid chloride and the hydroxyl groups of methoxy-PEG (2000 Da) in the presence of pyridine. The final polymer was purified by evaporating pyridine and washing with distilled water. For the 1%, and 20% PEG-grafted polymers (PEG1%-g-PLA, and PEG20%-g-PLA, respectively) the concentrations of D, L-lactide and allyl glycidyl ether were adjusted to give the desired ratios with the remaining synthesis procedure being the same. ^{1}H NMR spectra were recorded on a Brucker ARX 400 spectrometer (Bruker Biospin, Billerica, MA). Chemical shifts (δ) were measured in parts per million (ppm) using tetramethylsilane (TMS) as an internal reference. Gel permeation chromatography (GPC) was performed on a Water Associate chromatography system (Waters, Milford, MA) equipped with a refractive index detector and a Phenomenex Phenogel 5 μ column. Polystyrene standards were used for calibration with THF as the mobile phase at a flow rate of 0.6 mL/min.

2.3. Preparation of nanoparticles (NPs)

RHO loaded NPs were prepared by an O/W emulsion-solvent evaporation method. It should be mentioned that NPs were prepared using a 1:1 blend of high *M*w PLA (*M*w = 56,000 Da, Table 1) with each pegylated polymer, PEG-g-PLA of different PEG grafting density (1, 7, or 20% mol/mol of lactic acid monomer) to ensure high retaining ability of NPs for rhodamine B (RHO). RHO loaded NPs were prepared using an initial loading of 0.24% wt/wt of each polymer blend. Rhodamine (RHO) was first dissolved in the organic phase, 10 mL DCM followed by dissolution of each polymer blend (1 g) in the same phase. The organic phase was then emulsified into 30 mL PVA solution (0.5% w/v) as an external aqueous phase using high-pressure homogenizer (Emulsiflex C30, Avestin, Ottawa, Canada) at a pressure of 10,000 psi for 5 min. The O/W emulsion was collected by washing with another 30 mL 0.5% PVA. The DCM was evaporated under reduced pressure with constant stirring to obtain the NPs. Finally, NPs obtained as a suspension were then collected by centrifugation at 18,500 rpm for 30 min at 4 °C (Sorval® Evolution$_{RC}$, Kendro, USA), washed four times with distilled water, then lyophilized to obtain dry NPs (Freeze Dry System, Lyph.Lock 4.5, Labconco) and stored at 4 °C until further use. Small samples of the nanoparticle suspension were taken before lyophilization step in order to identify the original size of the particles obtained after homogenization and organic solvent evaporation.

Table 1
Polymer characterization by ^{1}H NMR and gel permeation chromatography (GPC).

Polymer	*Mn*[a] (Da)	*Mw*[a] (Da)	*Mw*/*Mn*[a]	PEG (mol%)[b]	*Mn* (^{1}H NMR)[b] (Da)
PLA	40,000	56,000	1.40	N/A	N/A
PEG1%-g-PLA	13,000	17,000	1.30	0.34%	9000
PEG7%-g-PLA	4000	8400	2.10	4.10%	8000
PEG20%-g-PLA	2200	2300	1.05	17.00%	4000

N/A not analyzed.
[a] Determined by GPC analysis using narrow molecular weight polystyrene standards.
[a] *Mw*/*Mn* = PDI of the polymers.
[b] Determined from the integration ratio of resonances due to PEG blocks at 3.64 ppm (–O–CH2–CH2–) and to the PLA blocks at 5.17 ppm ($^{Me-CH*<}$) in the ^{1}H NMR spectra.

2.4. Characterization of NPs

Size and size distribution of NPs were measured by dynamic light scattering (DLS) with a Malvern Autosizer 4800 instrument (Malvern Instruments, Worcestershire, UK) before and after lyophilization. DLS uses photon correlation spectroscopy to determine particle size from the temporal variation of light scattering caused by Brownian motion of the suspended particles. For all batches, fresh NP suspensions (0.1 mL) or lyophilized NPs (1 mg) were diluted 10 times with Milli-Q Water and size measurements were performed at 25 °C and scattering angle of 90°. The CONTIN program was used to extract size distributions from the autocorrelation functions. Measurements were performed in triplicate. The zeta potential of the nanoparticles was measured with Malvern ZetaSizer Nanoseries ZS (Malvern Instruments, Worcestershire, UK). Freeze dried NPs were suspended in 0.22 μm filtered 0.25% (w/v) saline solution (pH 7.4) and zeta potential was measured in triplicate. Nanoparticle morphology was studied using atomic force microscopy technique (AFM). AFM was performed with Nanoscope IIIa, Dimension™ 3100 (Digital Instruments, Santa Barbara, CA) in tapping mode. Samples were prepared by suspending the nanoparticles in water at a concentration of 10 mg/mL. These samples were deposited on freshly cleaved mica surface and were allowed to dry at room temperature. Subsequently, they were imaged in air at ambient conditions using etched silicon probes with tip radius of 5–10 nm and spring constant in the range of 20–100 N/m, oscillated at its fundamental resonant frequency (200–400 kHz).

2.5. Encapsulation efficiency (EE)

A weighed amount of NPs was dissolved into dichloromethane (DCM) followed by 5 min vortexing and then stirring for 1 h. Rhodamine (RHO) concentration was measured by spectrofluorimetry at excitation (λ_{ex}) and emission (λ_{em}) wavelengths of 552 and 585 nm, respectively, using a Tecan Safire plate reader (Durham, NC). Percent encapsulation efficiency (% EE) and percent drug loading (% DL) were calculated based on the following equations:

$$\%EE = \frac{\text{Drug entrapped in NPs}}{\text{Initial amount of drug added}} \times 100 \quad (1)$$

$$\%DL = \frac{\text{Drug entrapped in NPs}}{\text{Weight of NPs}} \times 100 \quad (2)$$

2.6. In vitro drug release study

All formulations prepared using different polymers were tested for in vitro release in triplicates in phosphate buffered saline (PBS, 10 mM, pH 7.4). 30 mg NPs were suspended in 10 mL PBS in a dialysis tubing (Spectra Por 1 membrane, 6–8 kDa cut-off). This dialysis tubing was placed in a screw-capped tube containing 40 mL PBS. The tubes were shaken at 200 rpm on a horizontal water bath shaker (Orbit Shaker Bath, Labline) maintained at 37 ± 0.5 °C. At predetermined time intervals, 15 mL of the external medium was withdrawn and replaced by fresh PBS to maintain sink conditions. The aliquots were assayed for the concentration of RHO released by spectrophotometry at 552 nm (U-2001 UV/Visible spectrophotometer, Hitachi).

2.7. Evaluation of protein adsorption to NPs surface

Dynamic light scattering (DLS) was used for measurement of the size of different NPs incubated with either 5% fetal bovine serum (FBS) or 2% bovine serum albumin (BSA). A weighed amount of NPs in 5 mL of either 5% FBS or 2% BSA was incubated at 37 °C for 24 h. Controls included the incubation of serum alone and RHO-loaded NPs alone with only distilled water for the same period of time. Samples were analyzed by DLS (n = 3) at the end of the incubation period to determine if there is any change in the size distribution pattern of different NPs.

2.8. Cell culture

Macrophage cell line, RAW 264.7 was grown in Dulbecco's modified Eagle cell culture medium (DMEM) containing 10% (v/v) heat-inactivated fetal bovine serum, 100 U/mL penicillin-G, and 100 mg/mL streptomycin (Invitrogen, Burlington, ON, Canada) in an atmosphere of 5% CO_2 and 95% relative humidity. The cells were routinely passaged at 90–95% confluence.

2.8.1. Evaluation of cellular toxicity of PEG-g-PLA NPs

Inhibition of cell proliferation was assessed by tetrazolium salt 3-(4,5-dimethylthiazol-2 yl)-2,5-diphenyl tetrazolium bromide (MTT) assay. Briefly, 1×10^5 RAW 264.7 cells were seeded in 96-well flat bottom plates (Costar, Corning, NY) and allowed to grow for 24 h. The cells were then incubated with increasing concentrations of each PEG-g-PLA NPs of different PEG grafting density for 24 h. Cell layers were washed with cold PBS and further incubated with 10 μL of MTT solution (5 mg/mL in PBS) for 4 h at 37 °C. Formazan crystals formed were then dissolved along with the cell layers and absorbance was measured on microplate reader at 570 nm. Cell viability was calculated with respect to PBS as control.

2.8.2. Cellular interaction with RAW 264.7: CLSM study

RAW 264.7 cells (a murine macrophage-like cell line) were seeded in eight-well chamber plate that contained a pre-sterilized coverslip at a concentration of 1×10^5 cells per well and allowed to adhere overnight in DMEM with 10% serum at 37 °C. Next day, the medium was removed; the cells were washed with a sterile Hanks balanced salt solution (HBSS). Then cells were incubated in RPMI 1640 medium with RHO-encapsulated nanoparticles (ensuring that rhodamine content is the same for all NPs batches based on the actual RHO loading) for 24 h at 37 °C. Next, the cells were washed six times with HBSS and were fixed with 4% paraformaldehyde solution. Coverslips were then mounted onto microscopy slides using Gel-Tol mounting medium (Thermo Scientific, Pittsburgh,

PA, USA) to protect the samples. Microscopy slides were observed with an inverted Olympus IX71 microscope (Olympus Canada Inc., Markham, ON) and an Evolution VF camera (MediaCybernetics, Bethesda, MD) with the same 60× objective lens and exposure time to allow comparison of measurements. Laser sources at 476, 488 and 496 nm were used to excite RHO and the fluorescence signal were detected in the 550–650 nm range. All microscopy gain and offset settings were maintained constant throughout the study. All images were processed with ImagePro software (MediaCybernetics, Bethesda, MD).

2.8.3. Cellular interaction with RAW 264.7: fluorimetry analysis

RAW 264.7 cells (1×10^5 cells/ well) were plated in 24-well flat bottom plates (Costar, Corning, NY) and allowed to adhere overnight in DMEM with 10% serum. Next day, the medium was removed and replaced by RPMI 1640 without serum. The cells were then incubated with different concentrations of RHO encapsulated NPs for 24 h at 37 °C. The cell monolayers were washed four times with cold PBS (pH 7.4) and then lysed with 0.2% Triton-X 100 in 0.2 N NaOH solution. The fluorescence was measured on microplate reader at excitation and emission wavelength of 552 and 585 nm, respectively. The amount of NPs phagocytosed was calculated from calibration curve of NPs under the same conditions.

2.9. Statistical analysis

Results were expressed as mean ± S.D. All data were generated in three independent experiments with two or three repeat. The *t*-test and the one-way analysis of variance (ANOVA) were performed to compare two or multiple groups, respectively. The difference between treatments was considered to be significant at a level of $P < 0.05$. Statistical analysis was performed for sizing, zeta potential, release, cellular uptake results, and encapsulation efficiency and loading data.

3. Results and discussion

Our previous development of PEG-g-PLA NPs with suitable drug delivery properties, e.g. small size, higher encapsulation efficiency, and prolonged release features led us to investigate the effect of PEG coating density on the physicochemical and in vitro macrophage uptake properties of the obtained NPs. We hypothesized that a high PEG coating density on the particles and a small particle size would improve the potential of PEG-g-PLA as a stealth carrier in vivo. The optimal PEG coverage density that could impart stealth behavior for the PEG-g-PLA NPs without compromising NPs properties was investigated in that study. With this purpose in mind, we synthesized PEG-g-PLA copolymers which differ in the PEG grafting density but have the same PEG chain length (2 kDa). Then, PEG-g-PLA nanoparticles of different PEG coating densities loaded with the fluorescent molecule rhodamine (RHO) were prepared as a tool for investigating NPs interaction with Raw 264.7 macrophage cell lines. The extent of cellular uptake of different particles was evaluated by fluorescence microscopy and fluorimetry analysis. RHO was chosen as the fluorescent label because it is more stable than fluorescein to quenching by light (Meng et al., 2006), efficiently entrapped and molecularly dispersed into NPs matrices (Esmaeili et al., 2008), easily loaded into NPs either by simple nanoprecipitation (Betancourt et al., 2009) or single o/w emulsion solvent/evaporation method (Cartiera et al., 2009). Moreover, the conditions required for obtaining good images for NPs inside the cells by fluorescence microscopy were found to be easily optimized with RHO use (Ishihara et al., 2008; Vila et al., 2004). To develop RHO loaded PEG-g-PLA NPs suitable for investigating the cellular interaction, NPs must show high retaining ability for the fluorescent marker. In order to achieve this, a 1:1 wt/wt polymer blend consisting of high *M*w PLA with each pegylated polymer, PEG-g-PLA of different PEG density (1, 7, or 20 mol%) was used to prepare NPs.

3.1. Characterization of polymers

PLA homopolymer and PEG-g-PLA copolymers of different PEG grafting densities were synthesized by ring-opening polymerization method. ^{1}H NMR spectroscopy and gel permeation chromatography (GPC) were used to measure the number average (*M*n) and weight average molecular weights (*M*w) of the synthesized polymers. The polydispersity was calculated by the ratio of *M*w to *M*n from the GPC data. GPC results are summarized in Table 1. All the synthesized polymers exhibited uniform molecular weight distribution as revealed by the narrow polydispersity index values as shown in the same table. Unimodal mass distribution ruled out the possibility of the presence of unreacted MePEG or poly(D, L-lactide) (data not shown). The molecular weight of PEG-g-PLA copolymer decreases with increasing grafting density of PEG. Similar finding was obtained before with PLA/PEG copolymer prepared by using different initial feed ratios for both PEG and PLA (Park and Kim, 2004). ^{1}HNMR spectra and chemical structure of PEG-g-PLA of different PEG grafting densities are shown in Fig. 1. A typical spectrum for all PEG-g-PLA polymers was obtained with a peak at 5.2 ppm corresponding to the tertiary PLA proton (m, –CH), a peak at 3.6 ppm for the protons of the repeating units in the PEG chain (m, OCH2–CH2O), and a peak at 1.5 ppm for the pendant methyl group of the PLA chain (m, –CH3). The grafting density of PEG over the PLA backbone was determined by comparing the integration ratio of resonances due to PEG blocks at 3.64 ppm (–O–CH2–CH2–) and to the PLA blocks at 5.17 ppm ($^{Me-CH^*}\diagdown$) in the ^{1}H NMR spectra. The actual grafting density of all synthesized polymers seems closer to the initial feed ratio as shown in Table 1. Also, it could be seen from Fig. 1 that the intensity of PLA peak at 5.2 ppm decreased remarkably upon increasing the grafting density and this might indicate the successful grafting of PEG over the PLA backbone.

3.2. NPs characterization

RHO loaded PEG-g-PLA nanoparticles were successfully prepared using an O/W emulsion solvent evaporation method by co-dissolving RHO and polymer blend (1:1 wt/wt PLA: PEG-g-PLA) in DCM and precipitating the polymer into nanoparticles in an aqueous phase having 0.5% PVA as a stabilizer after organic solvent evaporation. Table 2 summarizes the size distribution characteristics of RHO loaded PEG-g-PLA NPs of varying PEG densities (1, 7, and 20 mol%). For comparison, RHO loaded PLA was also included as the control. Particle size distribution by dynamic light scattering (DLS) showed unimodal distribution for freshly prepared NPs dispersion (before lyophilization) as well as lyophilized NPs. Freshly prepared NPs suspensions were found to be in the size range of 160–230 nm. Furthermore, a clear trend of decreasing the particle size was observed as their PEG content increased. Similar finding was obtained before with diblock copolymer PLA-PEG NPs (Sheng et al., 2009). The authors related that to the amphiphilic nature of PEG-PLA copolymers thus, reducing the interfacial tension between the aqueous and organic phases. Lyophilized NPs formulations showed larger particle size in the range of 300–400 nm compared to freshly prepared particles (Table 2). Thus, lyophilization process might induce particle aggregation. The size of the particles after freeze drying indicates that either a cryoprotectant or vigorous vortexing is needed to maintain the original size of the particles suspension. Vortexing for 5 min of a suspension of lyophilized NPs in Milli.Q water was successfully able to break the aggregate and reduce the size of the particles to almost its original size before lyophilization (Table 2). Particle size distribution data by

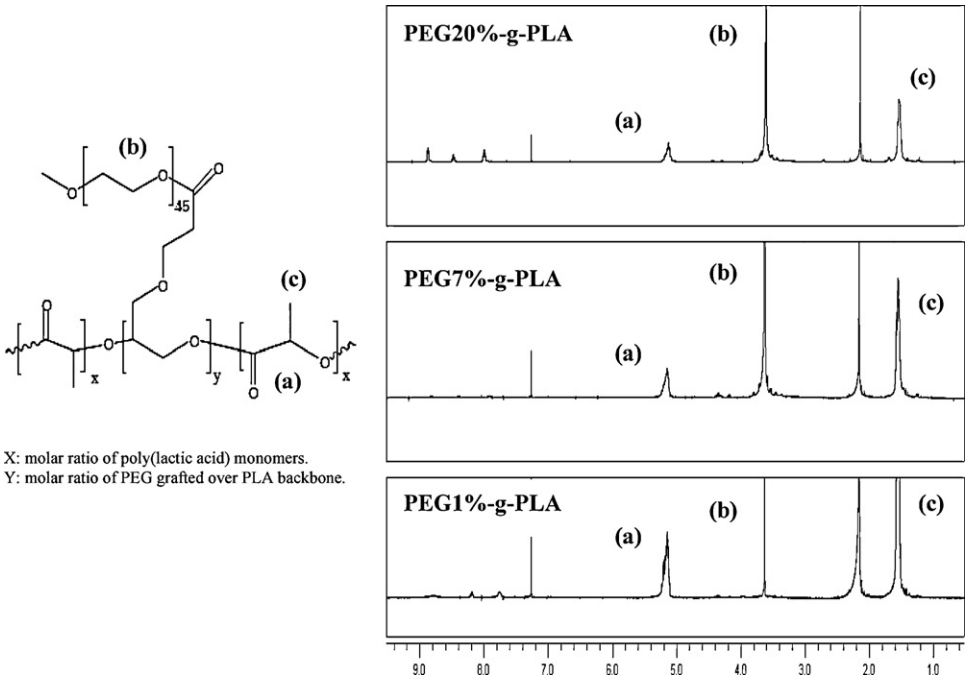

Fig. 1. [1]H NMR spectra and chemical structure of PEG-g-PLA copolymers of different PEG grafting densities over PLA backbone.

Table 2
Size distribution characteristics for different NPs after different stages of preparation.

NPs formulation	Size before Freeze drying (nm)[a,b]	PDI[c]	Size after freeze drying (nm)[a,b]	PDI[c]	Size after vortexing (nm)[a,b]	PDI[c]
PLA	224.0 ± 27	0.139	381.0 ± 30	0.178	270.0 ± 20	0.207
PEG1%-g-PLA	200.6 ± 28	0.002	318.0 ± 20	0.220	250.0 ± 41	0.161
PEG7%-g-PLA	185.6 ± 21	0.161	388.0 ± 14	0.078	230.0 ± 33	0.221
PEG20%-g-PLA	169.5 ± 23	0.092	380.9 ± 21	0.320	211.0 ± 23	0.159

[a] Median.
[b] All values indicate mean ± S.D. for $n = 3$ independent measurements for the same batch.
[c] Refers to polydispersity index.

DLS were also supplemented with a visual microscopic method like tapping mode atomic force microscopy (TM-AFM). Tapping mode atomic force microscopy (TM-AFM) is a versatile technique, which allows probing soft samples such as biological and polymeric materials (Kopp-Marsaudon et al., 2000; Raghavan et al., 2000). Fig. 2 displays TM-AFM images of RHO-loaded PEG7%-g-PLA nanoparticles before and after lyophilization. The nanoparticles suspension before lyophilization has a roughly spherical morphology and sizes in the range of 100 and 250 nm, with most particles having a diameter of less than 200 nm (Fig. 2(a)). While after lyophilization, it could be seen that particles showed some aggregating tendency confirming the size data obtained by DLS (Fig. 2(b)). AFM phase image analysis was also done to investigate the surface chemistry of the obtained particles as used before in our previous studies (Essa et al., 2010a,b). PEG7%-g-PLA NPs either before or after lyophilization showed the presence of an observable phase contrast at the surface of NPs revealed by some dark layers at the surface of bright cores (Fig. 2(a and b); right panels, P). These observations confirm the existence of PEG chains at the surface of PLA core. PEG-g-PLA NPs showed lower zeta potential values (close to zero) in comparison to the values reported before by other authors for PEG-b-PLA NPs (Beletsi et al., 2005; Govender et al., 2000; Gref et al., 2000) (Table 3). The greater reduction in zeta potential values of all PEG-g-PLA NPs of different PEG densities could be explained by the existence of a fraction of PVA at the surface of NPs (data not shown) which might have also played a role in masking the actual surface charge of PLA NPs. No significant difference in the zeta potential values of pegylated NPs of different PEG grafting densities was found (Table 3). This could also be explained by the same reason that the residual PVA chains at the NPs surface makes it difficult to estimate the real contribution of PEG coating density to surface charge reduction. What confirms this hypothesis that PLA NPs prepared by the same procedure also showed lower zeta potential values (−0.098 mV, Table 3) than expected (−40 mV) (Gref et al.,

Table 3
Other physicochemical characteristics for different NPs formulation.

NPs formulation	% EE[a]	% Lr (wt/wt)[b]	Zeta potential (mV)
PLA	10.01 ± 1.44	0.024 ± 0.003	−0.098 ± 3.78
PEG1%-g-PLA	31.11 ± 2.94	0.073 ± 0.007	0.273 ± 3.27
PEG7%-g-PLA	37.85 ± 0.97	0.090 ± 0.002	0.012 ± 3.72
PEG20%-g-PLA	67.79 ± 0.92	0.163 ± 0.002	0.003 ± 4.42

Targeted loading for all batches = 0.24% (wt/wt). All values indicate mean ± S.D. for $n = 3$ independent measurements.
[a] Refers to encapsulation efficiency.
[b] Refers to actual or real loading.

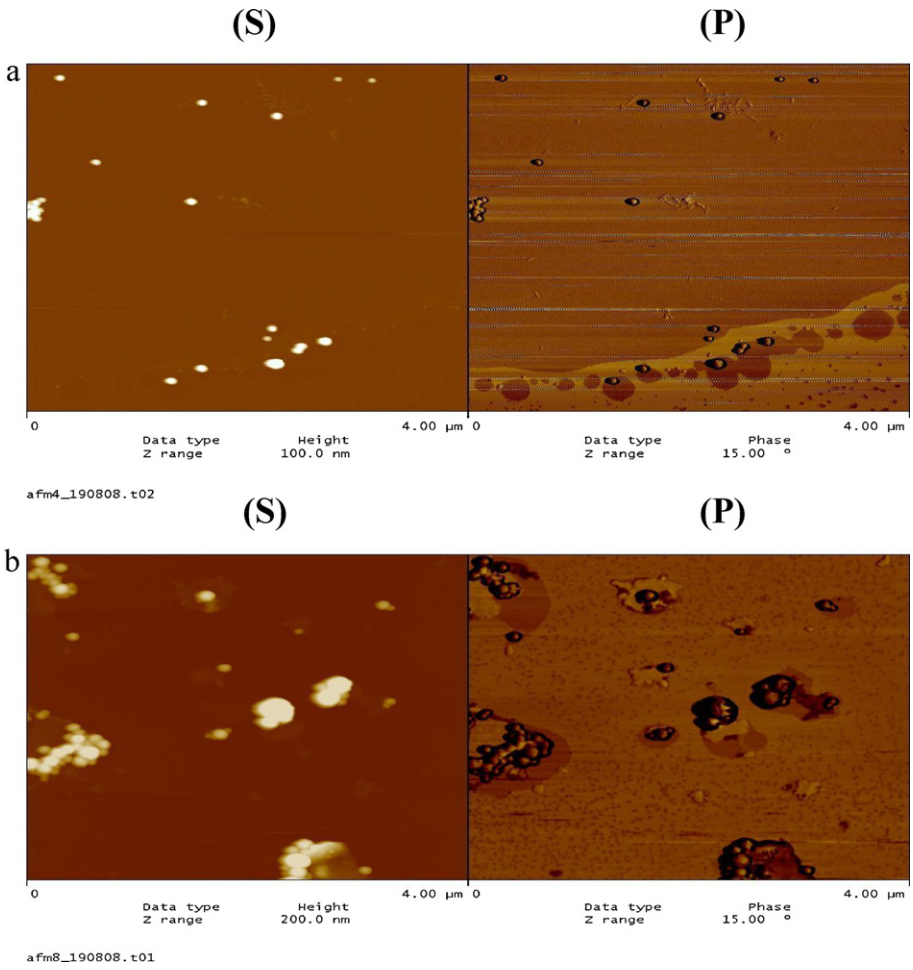

Fig. 2. AFM images of PEG7%-g-PLA NPs encapsulating rhodamine B (RHO), before (a) and after (b) lyophilization; surface morphology (left, S) and phase image (right, P).

2000; Musumeci et al., 2006; Peracchia et al., 1997). Zambaux et al. (1998) also reported a low zeta potential value of −4 mV for PLA NPs prepared with PVA as an emulsifier. The zeta potential findings confirm that residual PVA remained onto NPs surfaces was able to reduce the actual zeta potential values of either PLA or PLA modified NPs (PEG-g-PLA). This could be explained by the ability of PVA to be adsorbed efficiently (not removed by successive washing steps) onto the NPs surface masking the actual surface charge of PLA (resulted from COOH ionization).

3.3. Encapsulation efficiency (EE)

As seen from Table 3, % EE of RHO was found to be between 10% and 68% wt/wt depending on the polymer type. Grafted pegylated polymers showed better % EE than PLA homopolymer. The higher the grafting density, the more the encapsulation efficiency. The last finding could be attributed to the enhanced steric hindrance of the more mobile PEG chains existing at the surface of pegylated NPs, thus reducing premature diffusion of rhodamine into the external aqueous phase during solidification of the NPs. Although higher loading is readily possible since RHO favorably interacts with PLA, this was not necessary as the particles were already easily detected by fluorescence at the concentration levels tested. In a previous study by Sheng et al. (2009), haemoglobin (HbP) was encapsulated into PLA-PEG block copolymer of different PEG contents. The % EE of HbP was found to increase by increasing the PEG content. But further increase of PEG content to 20 wt% caused an obvious decrease of % EE. In our case, increasing the grafting density to 20 mol% resulted in further increase in the % EE. This could be explained by the difference in the polymer architecture between PEG-g-PLA copolymer used in our study compared to PEG-b-PLA. PEG-g-PLA NPs exhibited different PEG chain organization pattern than their corresponding block copolymer NPs as confirmed before by us (Essa et al., 2010a,b). PEG chains are easily oriented towards the surface of PEG-g-PLA NPs compared to PEG-b-PLA NPs. This leads to effective surface coverage in case of PEG-g-PLA NPs thus reducing the premature diffusion of drug towards the aqueous phase. While in PEG-b-PLA, some PEG chains might be interpenetrated inside the PLA core particularly at high PEG content (e.g. 20%), enhancing water uptake by the matrix, and hence, facilitating drug diffusion towards the external aqueous phase.

3.4. In vitro drug release

An in vitro release study was conducted in PBS at 37 °C in order to evaluate if the fluorescent marker (RHO) remains associated to the particles for a prudential period of time suitable for tracking NPs inside the cells. This could help us decide if RHO loaded NPs formulation were an optimal formulation for cellular uptake studies with RAW 264.7 cell lines. RHO release profile over a 15 days period is shown for particles made from different pegylated polymers compared to PLA homopolymer. RHO was released slowly from different NPs compared to RHO release from solution (Fig. 3). Specifically, within 15 h less than 20% of the agent had been released when incubated at 37 °C at pH 7.4. No significant difference in the release profile of NPs made from different PEG grating

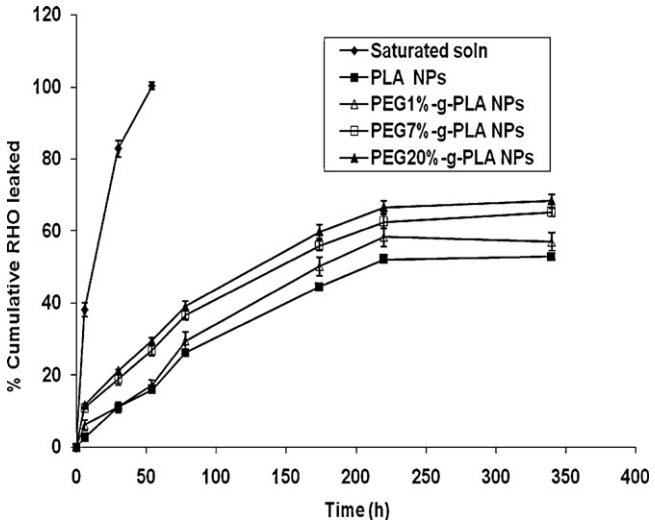

Fig. 3. In vitro release behavior of RHO from different PEG-g-PLA NPs in comparison to PLA NPs and RHO solution; values are represented as mean ± S.D. of three independent experiments.

densities was seen. This might indicate the ability of the high *M*w PLA added into each NPs formulation to efficiently trap and control RHO release over a prolonged period of time. Importantly, and as will be described in the cellular uptake section, controlled release of RHO over a time period of 24 h is more than sufficient for studying the interaction and uptake of nanoparticles by cells in vitro.

3.5. Plasma protein adsorption

It is well established that phagocytosis is a cellular phenomenon mainly initiated by the attachment of the foreign particles to the surface receptors of the phagocytic cells (Pratten and Lloyd, 1986). This phenomenon is facilitated by the adsorption of plasma proteins (opsonins) to the particle surface (Blunk et al., 1993; Moghimi and Patel, 1998). Therefore, DLS was used to investigate the possibility of plasma protein (PP) adsorption onto the NPs surface and whether there is any difference between different NPs batches in their ability to adsorb PP. This was simply done by monitoring the size distribution changes of NPs after incubation for a period of time with plasma proteins solution. DLS was used to determine the fate of RHO loaded PEG-g-PLA NPs of different PEG grafting densities, first, in the presence of 5% fetal bovine serum (5% FBS), and, second, in the presence of 2% bovine serum albumin (2% BSA). RHO loaded PLA NPs was also included for comparison. DLS analysis was performed on solutions of 5% FBS, RHO loaded NPs in distilled water and RHO loaded NPs in the presence of 5% FBS following incubation at 37 °C for 24 h. The same procedure was done with 2% BSA. DLS analysis of NPs in the presence of total serum is not possible as some blood proteins (i.e. immunoglobulins) form aggregates in aqueous solution. Size distribution analysis of 5% FBS solution revealed the presence of two size populations at ~10, and 66 nm (data not shown). Prior to incubation with 5% FBS the average diameter of all the investigated NPs was ranging from 200 to 260 nm (Fig. 4). After 24 h incubation with 5% FBS the average diameter of both PEG7%-g-PLA, and PEG20%-g-PLA NPs remained nearly unchanged. While PLA and PEG1%-g-PLA NPs showed clear aggregating tendency evidenced by the larger size and the broader polydispersity indices obtained after incubation with 5% FBS for 24 h (Fig. 4(a), and Fig. S1(a)). This might indicate that either PEG7%-g-PLA or PEG20%-g-PLA NPs did not adsorb significant quantities of plasma proteins compared to either PLA or PEG1%-g-PLA NPs. Bovine serum albumin (BSA) is the most abundant protein in serum. Many studies have shown

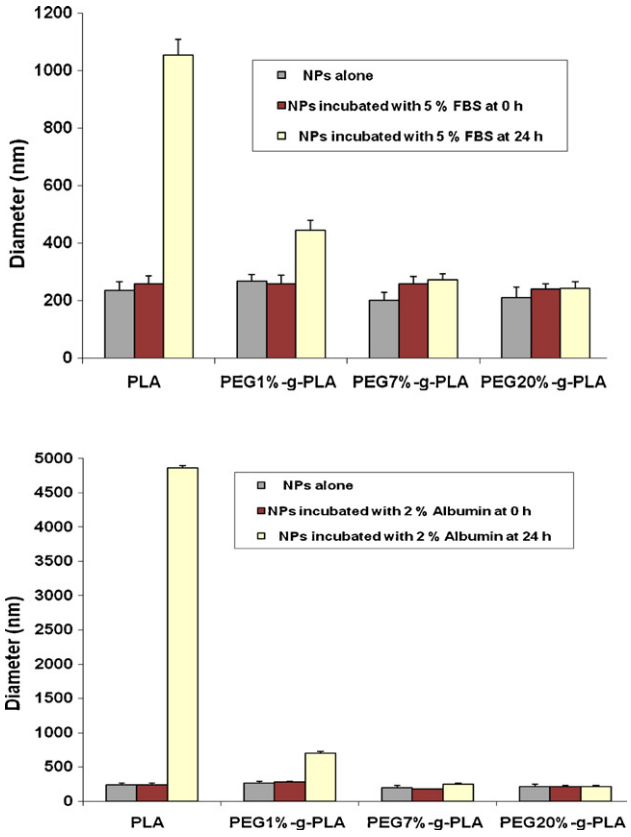

Fig. 4. (a) DLS size distribution data (nm) of different NPs upon incubation at 37 °C for 24 h with 5% FBS. (b) DLS size data (nm) of NPs upon incubation at 37 °C for 24 h with 2% BSA.

before that the major protein adsorped onto NPs surface is albumin (Allémann et al., 1997; Gref et al., 2000). DLS analysis of NPs incubated with 2% BSA was also done under the same conditions as before with 5% FBS. Size distribution analysis of 2% FBS solution revealed the presence of two size populations at ~2, and 18 nm (data not shown). And as found with 5% FBS, PLA and PEG1%-g-PLA NPs showed remarkable aggregating tendency evidenced by size distribution change after incubation with 2% BSA for 24 h (Fig. 4(b), and Fig. S1(b)]. These observations confirm that either PEG7%-g-

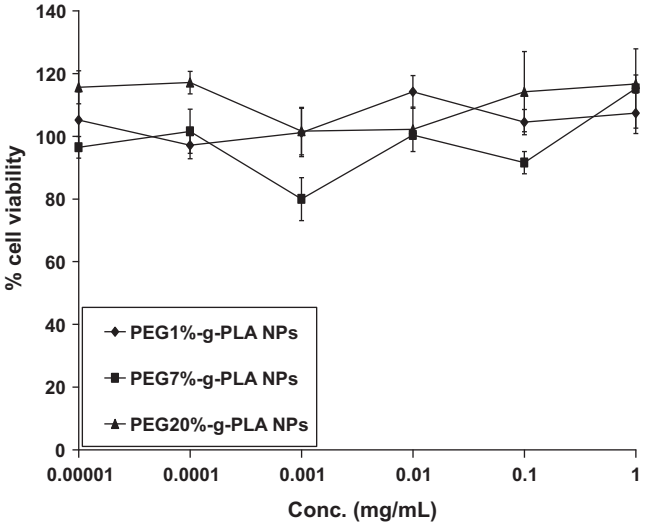

Fig. 5. Cytotoxicity of pegylated NPs of different PEG grafting densities over PLA backbone (1, 7, and 20% mol/mol) in RAW 264.7 cells by MTT assay.

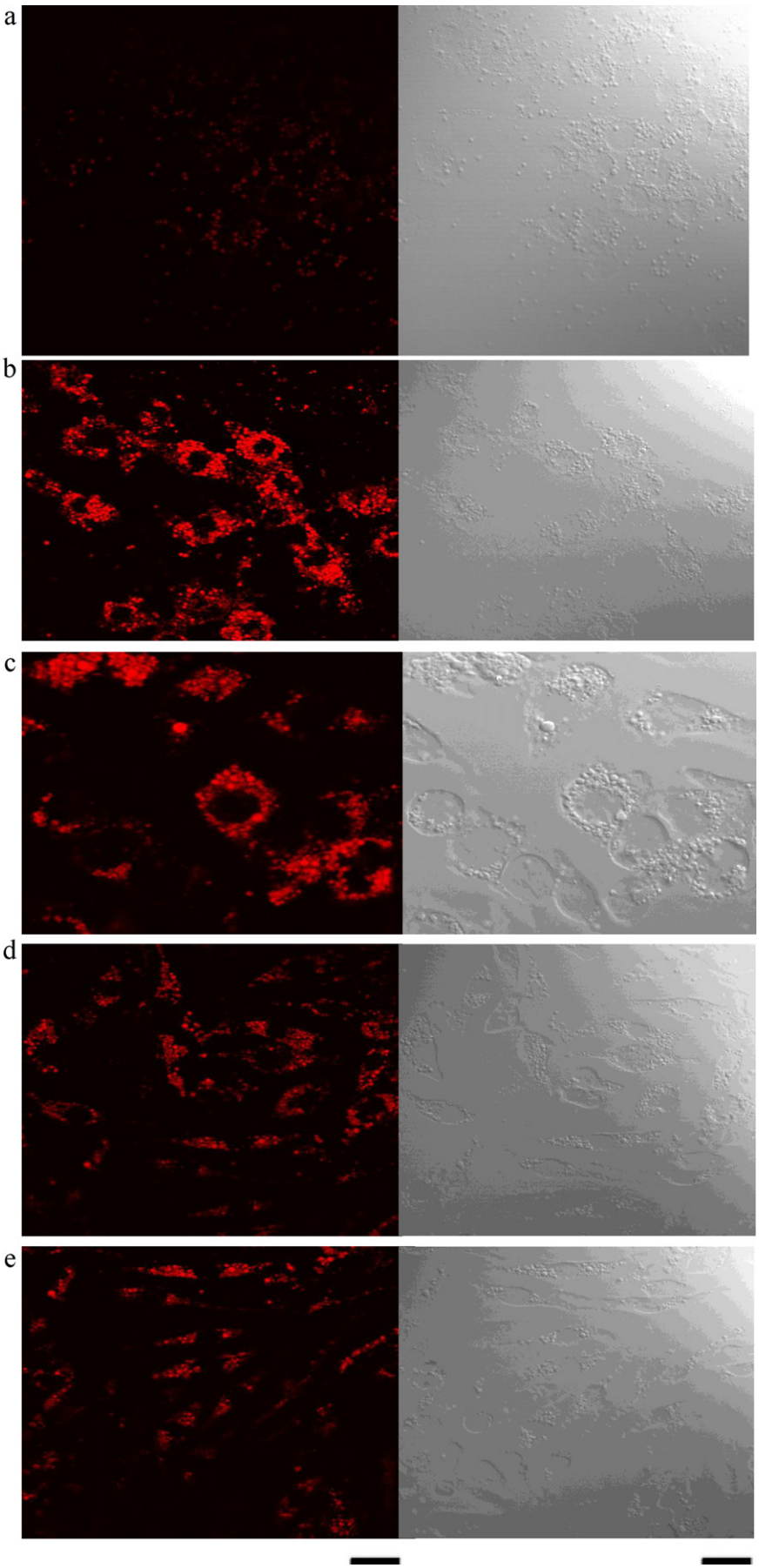

Fig. 6. Fluorescence images (right panels) and their corresponding phase contrast images (left panels) of RAW 264.7 cells after incubation with (a) RHO, (b) RHO loaded PLA NPs, (c) RHO loaded PEG1%-g-PLA NPs, (d) RHO loaded PEG7%-g-PLA NPs, and (d) RHO loaded PEG20%-g-PLA NPs. red images show RHO. Scale bar = 50 μm.

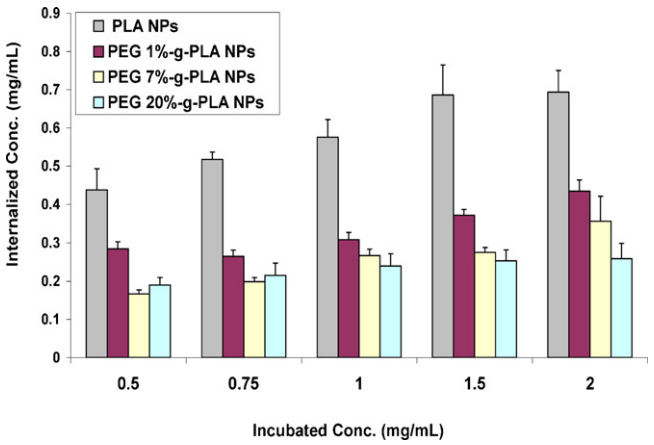

Fig. 7. RAW 264.7 cellular uptake of RHO encapsulated NPs made from PEG-g-PLA copolymer of different PEG grafting densities in comparison to PLA NPs. RAW 264.7 cells were incubated with NPs at 37 °C for 24 h.

PLA or PEG20%-g-PLA NPs could withstand the serum environment and that protein adsorption onto their surface occurs to a limited extent, if at all (Liu et al., 2005).

3.6. Cellular toxicity and uptake studies

PLA is a well-known biodegradable and biocompatible polymer. NPs made from PEG-g-PLA polymers of different PEG densities were well tolerated and exhibited no adverse effects on the cell viability as shown by cell proliferation assays (Fig. 5).

The interaction of RHO encapsulated nanoparticles with macrophage-like cells (RAW 264.7 cells) was first observed by fluorescence microscopy (Fig. 6). Microscopy studies showed that a higher fluorescence intensity, corresponding to higher RHO concentration, was observed in cells exposed to both RHO loaded PLA, and PEG1%-g-PLA nanoparticles (Fig. 6(b, and c, respectively)) compared to cells exposed to either RHO loaded PEG7%-g-PLA or PEG20%-g-PLA NPs (Fig. 6(d, and e, respectively)). This finding might indicate that nanoparticles made with PEG-g-PLA showed less internalization by macrophage cells than PLA nanoparticles. Moreover, to achieve sufficient masking by PEG on the surface of the nanoparticles, PEG grafting density higher than 1% is usually required to obtain lower internalization by macrophage cells.

To confirm the microscopy study results, estimation of the actual amount of NPs internalized after incubating RAW 264.7 cells for 24 h at 37 °C with different concentrations of RHO loaded NPs was investigated. Similar findings to microscopy results were obtained. Higher uptake was observed for PLA NPs as shown in Fig. 7. This is the result of the higher hydrophobicity of PLA NPs. Increasing the incubated conc, resulted in an increase in the actual amount internalized. It is interesting to note that PEG-g-PLA NPs of different PEG densities resulted in lower degree of internalization compared to PLA NPs in macrophages cell lines. It also could be seen that the higher the PEG grafting density, the lower the uptake of NPs by macrophage cells. This may be ascribed to surface hydrophilicity and neutral charge of the grafted copolymer NPs. These results are in accordance with other authors (Bazile et al., 1995; Prior et al., 2002; Verrecchia et al., 1995) who have reported that the higher the hydrophilicity of the surface, the lower the adsorption of plasma proteins onto them and hence lower macrophage uptake. However, increasing the grafting density from 7% to 20% did not show significant differences in their uptake ability indicating that the steric effect of PEG is concentration dependent (Mainardes et al., 2009).

4. Conclusions

In the present work, PEG-g-PLA copolymers of different PEG grafting density (1, 7, or 20% mol/mol of lactic acid monomer) were used to prepare nanoparticles loaded with the fluorescent agent RHO. These nanoparticles were designed as models for the study of particles uptake by RAW macrophage cells using confocal microscopy and fluorimetry analysis. An O/W emulsion solvent evaporation technique was utilized for preparation of nanoparticles. Spherical particles with sizes in the range of 150–250 nm were prepared with sufficient RHO encapsulation efficiency. Release studies revealed that RHO nanoparticles were optimal for cellular interaction studies because the agent is released at a very slow rate. DLS analysis for qualitatively studying the extent of plasma proteins adsorption to nanoparticle surface was also described and showed that PEG-g-PLA NPs might adsorb less amount of PP onto their surface. In vitro cellular studies with RHO nanoparticles revealed that PEG7%-g-PLA NPs showed less internalization by RAW cells as determined by confocal microscopy and fluorimetry analysis. PEG20%-g-PLA did not show significant difference in their phagocytosis tendency compared to PEG7%-g-PLA. The obtained results suggest the possibility of use of grafted copolymer PEG-g-PLA NPs can be used as long-circulating drug carriers for intravenous administration. The optimal PEG grafting density required to achieve that might vary from 4 to 7%. However, despite the promising ex vivo data, an actual in vivo data is needed to explore that indeed PEG-g-PLA NPs could exhibit stealth characteristics. A biodistribution study of Itraconazole loaded PEG-g-PLA NPs will be done in the future to support our preliminary data.

Acknowledgements

The work was supported in part by a grant of Fond Quebecois de la Recherche en Nature et Technologie (FQRNT). The authors wish to thank Prof. Jean François Bouchard, Ecole d'Optométrie, University of Montreal for his technical support using CLSM. Sherief Essa thanks the Ministry of Higher Education, Egypt for granting him a scholarship during his Ph.D.

Appendix A. Supplementary data

Supplementary data associated with this article can be found, in the online version, at doi:10.1016/j.ijpharm.2011.02.039.

References

Allémann, E., Gravel, P., Leroux, J.C., Balant, L., Gurny, R., 1997. Kinetics of blood component adsorption on poly(D, L-lactic acid) nanoparticles: evidence of complement C3 component involvement. J. Biomed. Mater. Res. 37, 229–234.
Bazile, D., Prud'homme, C., Bassoullet, M.-T., Marlard, M., Spenlehauer, G., Veillard, M., 1995. Stealth Me.PEG-PLA nanoparticles avoid uptake by the mononuclear phagocytes system. J. Pharm. Sci. 84, 493–498.
Beletsi, A., Panagi, Z., Avgoustakis, K., 2005. Biodistribution properties of nanoparticles based on mixtures of PLGA with PLGA-PEG diblock copolymers. Int. J. Pharm. 298, 233–241.
Betancourt, T., Shah, K., Brannon-Peppas, L., 2009. Rhodamine-loaded poly(lactic-co-glycolic acid) nanoparticles for investigation of in vitro interactions with breast cancer cells. J. Mater. Sci.-Mater. Med. 20, 387–395.
Blunk, T., Hochstrasser, D.F., Sanchez, J.C., Müller, B.W., Müller, R.H., 1993. Colloidal carriers for intravenous drug targeting: plasma protein adsorption patterns on surface-modified latex particles evaluated by two-dimensional polyacrylamide gel electrophoresis. Electrophoresis 14, 1382–1387.
Cartiera, M.S., Johnson, K.M., Rajendran, V., Caplan, M.J., Saltzman, W.M., 2009. The uptake and intracellular fate of PLGA nanoparticles in epithelial cells. Biomaterials 30, 2790–2798.
Cohen, H., Levy, R.J., Gao, J., Fishbein, I., Kousaev, V., Sosnowski, S., Slomkowski, S., Golomb, G., 2000. Sustained delivery and expression of DNA encapsulated in polymeric nanoparticles. Gene Ther. 7, 1896–1905.
Delie, F., Berton, M., Allémann, E., Gurny, R., 2001. Comparison of two methods of encapsulation of an oligonucleotide into poly(,-lactic acid) particles. Int. J. Pharm. 214, 25–30.

des Rieux, A., Fievez, V., Garinot, M., Schneider, Y.-J., Préat, V., 2006. Nanoparticles as potential oral delivery systems of proteins and vaccines: a mechanistic approach. J. Control. Rel. 116, 1–27.
Esmaeili, F., Ghahremani, M.H., Esmaeili, B., Khoshayand, M.R., Atyabi, F., Dinarvand, R., 2008. PLGA nanoparticles of different surface properties: preparation and evaluation of their body distribution. Int. J. Pharm. 349, 249–255.
Essa, S., Rabanel, J.M., Hildgen, P., 2010a. Effect of aqueous solubility of grafted moiety on the physicochemical properties of poly(D, L-lactide) (PLA) based nanoparticles. Int. J. Pharm. 388, 263–273.
Essa, S., Rabanel, J.M., Hildgen, P., 2010b. Effect of polyethylene glycol (PEG) chain organization on the physicochemical properties of poly(D, L-lactide) (PLA) based nanoparticles. Eur. J. Pharm. Biopharm. 75, 96–106.
Govender, T., Riley, T., Ehtezazi, T., Garnett, M.C., Stolnik, S., Illum, L., Davis, S.S., 2000. Defining the drug incorporation properties of PLA-PEG nanoparticles. Int. J. Pharm. 199, 95–110.
Govender, T., Stolnik, S., Garnett, M.C., Illum, L., Davis, S.S., 1999. PLGA nanoparticles prepared by nanoprecipitation: drug loading and release studies of a water soluble drug. J. Control. Rel. 57, 171–185.
Gref, R., Lück, M., Quellec, P., Marchand, M., Dellacherie, E., Harnisch, S., Blunk, T., Müller, R.H., 2000. 'Stealth' corona-core nanoparticles surface modified by polyethylene glycol (PEG): influences of the corona (PEG chain length and surface density) and of the core composition on phagocytic uptake and plasma protein adsorption. Colloids Surf. B: Biointerfaces 18, 301–313.
Hans, M.L., Lowman, A.M., 2002. Biodegradable nanoparticles for drug delivery and targeting. Curr. Opin. Solid State Mater. Sci. 6, 319–327.
Ishihara, T., Takahashi, M., Higaki, M., Takenaga, M., Mizushima, T., Mizushima, Y., 2008. Prolonging the in vivo residence time of prostaglandin E-1 with biodegradable nanoparticles. Pharm. Res. 25, 1686–1695.
Kopp-Marsaudon, S., Leclere, P., Dubourg, F., Lazzaroni, R., Aime, J.P., 2000. Quantitative measurement of the mechanical contribution to tapping-mode atomic force microscopy images of soft materials. Langmuir 16, 8432–8437.
Leo, E., Brina, B., Forni, F., Vandelli, M.A., 2004. In vitro evaluation of PLA nanoparticles containing a lipophilic drug in water-soluble or insoluble form. Int. J. Pharm. 278, 133–141.
Liu, J., Zeng, F., Allen, C., 2005. Influence of serum protein on polycarbonate-based copolymer micelles as a delivery system for a hydrophobic anti-cancer agent. J. Control. Rel. 103, 481–497.
Magjarevic, R., Ling, Y., Huang, Y., 2008. Preparation and release efficiency of poly (lactic-co-glycolic) acid nanoparticles for drug loaded paclitaxel. In: Peng, Y., Weng, X. (Eds.), 7th Asian-Pacific Conference on Medical and Biological Engineering, vol. 19. Springer, Berlin, Heidelberg, pp. 514–517.
Mainardes, R.M., Gremiao, M.P., Brunetti, I.L., da Fonseca, L.M., Khalil, N.M., 2009. Zidovudine-loaded PLA and PLA-PEG blend nanoparticles: influence of polymer type on phagocytic uptake by polymorphonuclear cells. J. Pharm. Sci. 98, 257–267.
Meng, W., Parker, T.L., Kallinteri, P., Walker, D.A., Higgins, S., Hutcheon, G.A., Garnett, M.C., 2006. Uptake and metabolism of novel biodegradable poly (glycerol-adipate) nanoparticles in DAOY monolayer. J. Control. Rel. 116, 314–321.
Moghimi, S.M., Patel, H.M., 1998. Serum-mediated recognition of liposomes by phagocytic cells of the reticuloendothelial system – the concept of tissue specificity. Adv. Drug Deliv. Rev. 32, 45–60.
Mohanraj, V.J., Chen, Y., 2007. Nanoparticles – A Review. Association of Crop Science, Uganda.
Musumeci, T., Ventura, C.A., Giannone, I., Ruozi, B., Montenegro, L., Pignatello, R., Puglisi, G., 2006. PLA/PLGA nanoparticles for sustained release of docetaxel. Int. J. Pharm. 325, 172–179.
Nadeau, V., Leclair, G., Sant, S., Rabanel, J.-M., Quesnel, R., Hildgen, P., 2005. Synthesis of new versatile functionalized polyesters for biomedical applications. Polymer 46, 11263–11272.
Panyam, J., Labhasetwar, V., 2003. Biodegradable nanoparticles for drug and gene delivery to cells and tissue. Adv. Drug Deliv. Rev. 55, 329–347.
Park, S.-J., Kim, S.-H., 2004. Preparation and characterization of biodegradable poly(L-lactide)/poly(ethylene glycol) microcapsules containing erythromycin by emulsion solvent evaporation technique. J. Colloid Interface Sci. 271, 336–341.
Peracchia, M.T., Gref, R., Minamitake, Y., Domb, A., Lotan, N., Langer, R., 1997. PEG-coated nanospheres from amphiphilic diblock and multiblock copolymers: investigation of their drug encapsulation and release characteristics. J. Control. Rel. 46, 223–231.
Pratten, M.K., Lloyd, J.B., 1986. Pinocytosis and phagocytosis: the effect of size of a particulate substrate on its mode of capture by rat peritoneal macrophages cultured in vitro. Biochim. Biophys. Acta, Gen. Subj. 881, 307–313.
Prior, S., Gander, B., Blarer, N., Merkle, H.P., Subirá, M.L., Irache, J.M., Gamazo, C., 2002. In vitro phagocytosis and monocyte-macrophage activation with poly(lactide) and poly(lactide-co-glycolide) microspheres. Eur. J. Pharm. Sci. 15, 197–207.
Raghavan, D., Gu, X., Nguyen, T., VanLandingham, M., Karim, A., 2000. Mapping polymer heterogeneity using atomic force microscopy phase imaging and nanoscale indentation. Macromolecules 33, 2573–2583.
Sheng, Y., Yuan, Y., Liu, C., Tao, X., Shan, X., Xu, F., 2009. In vitro macrophage uptake and in vivo biodistribution of PLA-PEG nanoparticles loaded with hemoglobin as blood substitutes: effect of PEG content. J. Mater. Sci.-Mater. Med. 20, 1881–1891.
Soppimath, K.S., Aminabhavi, T.M., Kulkarni, A.R., Rudzinski, W.E., 2001. Biodegradable polymeric nanoparticles as drug delivery devices. J. Control. Rel. 70, 1–20.
Verrecchia, T., Spenlehauer, G., Bazile, D.V., Murry-Brelier, A., Archimbaud, Y., Veillard, M., 1995. Non-stealth (poly(lactic acid/albumin)) and stealth (poly(lactic acid-polyethylene glycol)) nanoparticles as injectable drug carriers. J. Control. Rel. 36, 49–61.
Vila, A., Gill, H., McCallion, O., Alonso, M.J., 2004. Transport of PLA-PEG particles across the nasal mucosa: effect of particle size and PEG coating density. J. Control. Rel. 98, 231–244.
Wang, M.D., Shin, D.M., Simons, J.W., Nie, S., 2007. Nanotechnology for targeted cancer therapy. Expert Rev. Anticancer Ther. 7, 833–837.
Zambaux, M.F., Bonneaux, F., Gref, R., Maincent, P., Dellacherie, E., Alonso, M.J., Labrude, P., Vigneron, C., 1998. Influence of experimental parameters on the characteristics of poly(lactic acid) nanoparticles prepared by a double emulsion method. J. Control. Rel. 50, 31–40.